ACS APPLIED MATERIALS & INTERFACES

Research Article

www.acsami.org

Pulsed-Laser Deposited Transition-Metal Carbides for Field-Emission Cathode Coatings

Tyson Back,*[,†,‡] Steven B. Fairchild,[†] Kent Averett,[†] Benji Maruyama,[†] Neal Pierce,[†,‡] Marc Cahay,[§] and P. Terrence Murray[†,‡]

[†]Air Force Research Laboratory, Materials and Manufacturing Directorate, Wright-Patterson Air Force Base, 3005 Hobson Way, Ohio 45433, United States

[‡]University of Dayton Research Institute, 300 College Park, Dayton, Ohio 45469-0170, United States

[§]School of Electronics and Computing Systems, University of Cincinnati, 812C Rhodes Hall, Cincinnati, Ohio 45221, United States

Supporting Information

ABSTRACT: Thin films of transition-metal carbides ZrC, HfC, and TiC were deposited by pulsed-laser deposition under vacuum. The surface chemistry of the films was characterized with ultraviolet photoelectron spectroscopy, X-ray photoelectron spectroscopy, and Auger electron spectroscopy in situ. X-ray diffraction was used to characterize the film structure. TiC was shown to be nearly stoichiometric and polycrystalline. The TiC was applied to a vertically aligned carbon nanotube sample and characterized by field emission. Field-emission results showed enhanced current and current density at a film thickness, 5 nm, not previously reported in the literature. Emission from TiC films was also shown to be less affected by adsorbates during field emission. Pulsed-laser deposition of TiC offers a distinct advantage over other techniques in that high-quality films can be obtained under ultrahigh vacuum conditions without the use of a reactive background gas or excessively high annealing temperatures. The application of TiC by pulsed-laser deposition as a cathode coating shows potential for integration into a fabrication process.

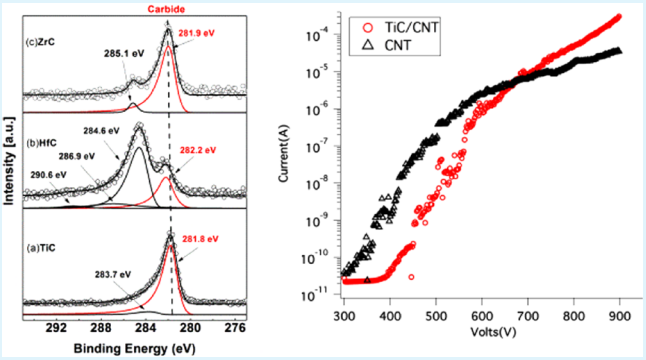

KEYWORDS: *carbide, surface analysis, carbon nanotubes, field emission, transition metals, coatings*

INTRODUCTION

Transition-metal carbide(s) (TMC(s)) make an ideal candidate for field-emission (FE) applications. TMCs are wear resistant, electrically conductive, stable at high temperatures, resistive to oxidation environments, and have relatively low work functions. For FE applications, TMCs also have the added benefit of being resistant to ion back-bombardment in FE devices. Ion back-bombardment can degrade field-emission cathodes, thereby shortening their lifetime. Application of these materials for use in an FE device occurs in one of two ways: either as a bulk material with a geometry appropriate for a field-emission tip or as a thin coating applied to an existing field-emission cathode.

Senzaki and Kumashiro[1] were one of the first to use titanium carbide as a field-emission cathode. A work function as low as 2.6 eV was extracted from field-emission microscopy measurements after a high-temperature anneal under vacuum. Fujii et al.[2] also used field-emission microscopy to show the effects of the annealing temperature and the background gas environment on TiC field-emission tips. Stable emission patterns were obtained after annealing at 1900 °C. Oxygen was shown to increase current fluctuations as its partial pressure was increased. Exposure to hydrogen was shown to cause the smallest fluctuations in current. These results suggest that partial pressures of gases present during field emission can play a significant role in cathode stability.

Mackie et al.[3−8] and Charbonnier et al.[9,10] have investigated the use of TMCs for cathodes in field and thermionic emission extensively. In all cases, the TMC emitters were shown to have low work functions and stable emission. For the study of bulk emitters, the TMCs were typically fabricated by a floating zone arc refinement method.[11] This meant that tips were exposed to atmosphere before being placed under vacuum, and an annealing process was necessary. In most cases, temperatures above 1000 °C were required to remove contaminants from the surface. Such high annealing temperatures can cause a restructuring of the tip, which could result in a reduction in the total current from the tip and may not be feasible with a working device.

One way to avoid the high temperature cleaning procedure is to produce FE tips in situ. Unfortunately, none of the standard techniques for making bulk TMC cathodes make this a realistic option for device fabrication. Charbonnier et al.[10] explored the

Received: August 12, 2013
Accepted: August 29, 2013
Published: August 29, 2013

use of thin carbide coatings. HfC and ZrC were e-beam evaporated onto Si and Mo FE tips and arrays in situ. This approach had the advantage of being able to determine the effects of a clean carbide surface that had not been subjected to high temperatures. The results showed that the thin films of HfC and ZrC reduced the work function of the tips and arrays. The films also showed a work function dependence on the substrate, suggesting that substrate−coating interactions could play an important role in cathode performance.

Applying TMCs as a coating to improve FE performance has also been investigated for use in carbon nanotube (CNT) cathodes. The use of CNTs as field emitters has been shown to have great promise for areas such as electron microscopy and field-emission displays.[12] Pan et al.[13] demonstrated a 2 orders of magnitude improvement in the FE of CNT arrays by the application of a 1 nm coating of TiC. Uh et al.[14] showed that Ti coatings on CNTs resulted in a lower turn-on voltage, higher emission current density, and improved emission uniformity when compared to noncoated CNT samples. Qin and Hu[15] reported similar results by depositing a metal film on the CNTs and annealing at 900 °C.

Previously cited works demonstrated the feasibility of applying TMC coatings for FE applications. These coatings were typically applied by e-beam evaporation, and few attempts were made to characterize the surface chemistry[6] of the films in situ. It is the purpose of this Article to describe the use of TMCs applied by pulsed-laser deposition (PLD) for use with field-emission cathodes. The PLD of TMC coatings are typically formed with reactive background gases such as hydrocarbons. The use of hydrocarbon gases can result in a surface rich in amorphous carbon, which is not desirable. For FE cathodes, the first few monolayers of a deposited film can have a significant impact on performance and are of primary concern. As a result, TiC, ZrC, and HfC were deposited onto substrates under vacuum. The electronic properties of these films were analyzed in situ without exposure to air. Analyses of the films were investigated with X-ray photoelectron spectroscopy (XPS), Auger electron spectroscopy (AES), and ultraviolet photoelectron spectroscopy (UPS). X-ray diffraction data was acquired ex situ to determine the structure of the films. These characterization methods allow a comparison to be made between the surface of the films and the bulk material.

EXPERIMENTAL SECTION

Substrate samples consisted of *p*-type ⟨100⟩ silicon wafers and vertically aligned carbon nanotubes (VACNTs). The planar Si wafers and VACNTs substrates were used for surface and field-emission analysis, respectively. Before deposition, silicon wafers were rinsed with copious amounts of acetone and methanol and were immediately placed under vacuum. Depositions were carried out in the antechamber of a surface-analysis system. The background pressure in the antechamber reached 2.0×10^{-8} Torr or less before deposition. Depositions in the antechamber made it possible to probe the surface in situ without exposure to air. The PLD target was positioned normal to the substrate with a target-to-substrate distance of about 5 cm.

An excimer laser with a wavelength of 248 nm and pulse width of 25 ns was used for the ablation of the targets. The laser was pulsed at 10 Hz for all depositions. During ablation, the operating pressure ranged from 1.0×10^{-7} to 3.0×10^{-7} Torr. A CO_2 laser (10.6 μm) was used to heat the substrate. The heating laser struck the substrates from the backside, and the temperature was monitored with an optical pyrometer from the front side. The temperature of all substrates was 750 °C during deposition. The deposition rates of all three TMC targets were measured with a quartz crystal thin-film deposition monitor, which yielded a deposition rate of 0.1 Å/s. The depositions were carried out for 500 s, resulting in a 5 nm coating. The same deposition conditions were used for all substrates.

Data were collected in situ with a Staib surface-analysis instrument equipped with a DESA 150 analyzer. The background pressure in the analysis chamber was less than 3.0×10^{-10} Torr. The instrument was capable of collecting XPS, AES, and UPS measurements. XPS data were collected with a standard Mg Kα (1253.6 eV) excitation source. The energy scale was calibrated against Au $4f_{7/2}$ and Cu $2p_{3/2}$ at binding energies of 84.0 and 932.6 eV, respectively. The XPS resolution was determined by the fwhm of the Au $4f_{7/2}$ line, which was found to be 1.2 eV. The pass energies for survey and high-resolution scans were 80 and 20 eV, respectively. Auger scans were recorded in undifferentiated mode at a resolution of 0.2%. For UPS, the He I (21.2 eV) line was generated with a differentially pumped Specs 10/35 He discharge lamp. The Fermi edge was calibrated against a sputter-cleaned gold sample. The resolution, obtained from the width of the Fermi edge, was determined to be 300 meV. UPS data were collected with a negative bias applied to the substrate to obtain the true work function of the deposited film.

XPS data were background corrected with the Shirley[16] background, and the components were fitted to each spectrum using a Levenberg−Marquardt algorithm that minimizes χ^2. Each component consists of a convolution of the Gaussian and Lorenztian functions. The photoemission intensities were corrected to account for Scofield cross sections, kinetic energy, and analyzer transmission function. Auger data were differentiated with a Savitzky−Golay[17] routine using five data points.

The X-ray diffraction measurements were performed in the Bragg−Brentano parafocusing geometry on a PANalytical X'Pert Pro MRD system using the 4 in. wafer stage. The incident beam optics consisted of a Cu Kα source operated at 45 kV and 40 mA. The diffracted beam optics consisted of a 0.18° parallel plate collimator with a 0.04 rad Soller slit and a scintillation detector. 2θ scans were acquired for all samples with an incident angle of 7°.

Vertically aligned multiwalled carbon nanotubes (VACNTs) were grown on a substrate via thermal chemical-vapor deposition in a 2″ diameter tube furnace. The tube furnace was capable of rapid sample insertion via a transfer arm to minimize catalyst coarsening.[18] The catalyst support consisted of a 10 nm layer of Al_2O_3 deposited by atomic layer deposition (ALD) on a 250 nm thermal SiO_2 on a Si wafer. The use of an alumina support layer is common in VACNT growth because it leads to increased nucleation density. A catalyst layer of 0.6 nm Fe was then deposited by ion-beam sputtering. The supported catalyst was placed in a load lock, and both the load lock and the furnace were pumped to a base pressure of $\sim 10^{-7}$ Torr and heated from room temperature to the synthesis temperature of 780 °C at a 25 °C/min ramp rate. Upon reaching the synthesis temperature, the furnace was brought to atmospheric pressure by backfilling with Ar. Mass flow controllers from MKS Instruments were then used to establish gas flows of 550 sccm Ar, 425 sccm H_2, and 25 sccm C_2H_4 into the furnace. The gases were obtained from Airgas, Inc. with the following purity: Ar 99.9997%, H_2 99.9999%, and C_2H_4 99.9%. The temperature and gas flow was allowed to reach steady state (~10 min), and the supported catalyst was then inserted into the hot zone of the furnace for 30 min.

After growth, the CNT sample was placed in a custom built field-emission system. The sample was pumped in a load lock until the pressure reached 1.0×10^{-7} Torr. The sample was then transferred into the field-emission chamber, which maintained a background pressure of 5.0×10^{-9} Torr. A copper anode probe tip with a diameter of 750 μm was centered over the CNT sample. The centering of the anode tip over the sample was accomplished with the use of two optical cameras looking through two different windows on the chamber. The cameras were placed approximately 90° from each other in a plane perpendicular to the FE axis. An Infinity SK Long Distance Microscope with a C4 objective was used for imaging the fiber cathode and the anode−cathode gap distance. Once the gap distance was set to 100 μm, the voltage on the anode was ramped at 2 V/step, 10s/step, from 300 to 900 V with a Kiethley 6517A source meter. The voltage range was selected to avoid thermal effects at high field strengths. Data

was recorded at each voltage by a computer running LabView. Increasing the voltage in this manner allows the sample to outgas properly. We have found that emission from the cathode is much more stable when an outgassing procedure is used.

The CNT sample was then placed in the surface analysis system where it was pumped to pressure of 2.0×10^{-8} Torr or greater. The CNT substrate was then heated with a CO_2 laser (10.6 μm) from the backside of the substrate to a temperature of 750 °C. The temperature was measured with an optical pyrometer from the front side of the sample. The CNT sample was then coated with TiC in the same manner as the planar Si substrates. After the coating was applied, the CNT sample was allowed to cool to room temperature and immediately placed in the FE system. The coated sample was run again under the same FE conditions as previously described.

RESULTS AND DISCUSSION

Figure 1 shows the in situ UPS results from HfC, ZrC, and TiC. The secondary edge from all three spectra was used to determine the work function of the films. The expanded region clearly shows TiC to have the lowest work function of the three films. A work function of 3.8 eV agrees well with values reported in the literature.[19] ZrC and HfC had values of 4.0 and 4.5 eV, respectively. These values are higher than what was reported previously.[10,20] This suggests that the ZrC and HfC surface do not consist purely of the carbide phase. For ZrC, we cannot rule out the possibility of Zr metal present on the surface resulting in the observed work function. The same cannot be said for the HfC film because the metal has a significantly lower work function, 3.9 eV, than what was observed experimentally. The XPS results, Figure 2, shed light on the work function differences between the three films.

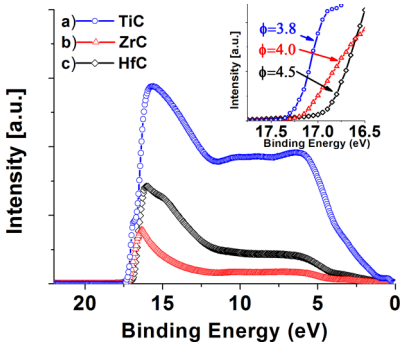

Figure 1. UPS results from the (a) TiC, (b) ZrC, and (c) HfC. The inset shows work function values as determined from the onset of each secondary edge.

Figure 2 shows the C 1s region for TiC, HfC, and ZrC. The TiC results were fit with two peaks. The peak at 281.8 eV agrees well with the previous published literature for PLD TiC films.[21,19] A small peak at 283.7 eV is also present and is most likely associated with physisorbed carbon on titanium. Similar binding energies were reported with carbon deposition on gold[22] as well as TiC nanocomposites.[23,24] Figure 2b shows the same region for HfC. A carbide bond is attributed to the peak at 282.2 eV. This value is slightly higher than what was reported in the literature.[25] Another peak at 284.6 eV dominates this region and is most likely the result of graphitic carbon present in the film. This agrees well with the UPS results from Figure 1 that showed a work function of 4.5 eV. This value is close to what one would find for graphitic carbon.[26] Figure 2c shows results from the ZrC film. A carbide peak is also present at 281.9 eV. Another peak is also present at 285.1 eV, which

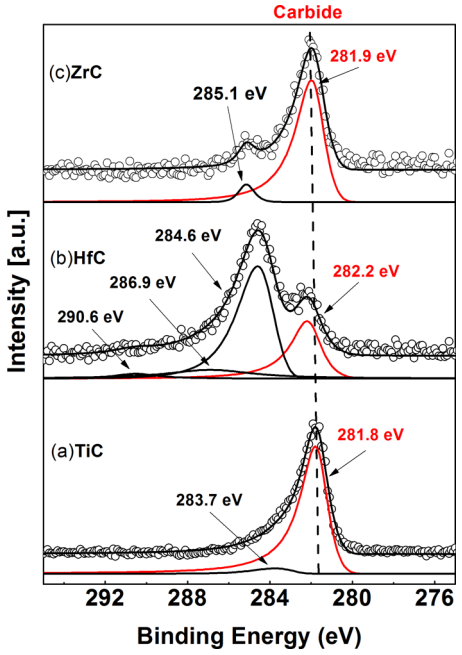

Figure 2. XPS results from the (a) TiC, (b) HfC, and (c) ZrC depositions. The black dotted line shows approximately where the carbide binding energies occur for each film. The sum curves of all fitted components are overlaid with the experimental data (solid black lines). The fitted components are offset from the experimental for display purposes. All carbide components are displayed in red. The carbide binding energies for TiC, HfC, and ZrC are 281.8, 282.2, and 281.9 eV, respectively.

suggests the presence of amorphous carbon. The presence of amorphous carbon and/or Zr metal is most likely the reason for the slightly higher work function for ZrC shown in Figure 1.

Table 1 shows the quantitative results of the C 1s region for all three carbides from Figure 2. TiC and ZrC have substoichiometric concentrations. Group IV and V carbides have been known to have carbon vacancies, which cause them to be nonstoichiometric.[27] These nonstoichiometric structures are quite stable, and for the case of TiC_x, x can vary anywhere from 0.55 to 1.0.[27] For ZrC and TiC, chemical shifts in the metal region caused by a metal−carbon bond make it easily distinguishable from a purely metallic peak in their respective atomic core-level transition regions. Spectra from the Zr 3d and Ti 2p regions, data not shown, suggest that only the carbide is present on the surface of the film. In the case of HfC, fitting the components in the Hf 4f region proved to be difficult. The binding energy of the Hf 4f metal transition is nearly identical to the binding energy of the Hf 4f carbide peak that resolving the two chemical states[28] is ambiguous given the resolution capabilities of our instrument. Also, the carbon valence band spectra overlaps[29,30] with the Hf 4f region, making an accurate determination of the hafnium and carbon stoichiometries difficult. As can be seen in Table 1, the hafnium/carbon ratio

Table 1. Quantitative XPS Results of Metal/Carbon Ratios for Each Transition-Metal Carbide Film

TMC	x
HfC_x	1.69
ZrC_x	0.74
TiC_x	0.98

dx.doi.org/10.1021/am403362w | ACS Appl. Mater. Interfaces 2013, 5, 9241−9246

appears to be over stoichiometric. This ratio could also be due to the formation of metallocarbohedrenes[31,32] on the surface of the HfC films.

The HfC C 1s region also shows a significant amount of graphitic carbon as well as much smaller amount of amorphous carbon. The noncarbidic carbon present in the film could originate from excess carbon in the ablation target. All of the TMC targets used in this study were fabricated by hot isostatically pressing a metal-carbide powder. This process typically creates grains in the material that can vary between several micrometers up to millimeters. We reason that the HfC target with the highest melting temperature of all of the TMCs studied has the smallest grains. The small grains size will result in a high concentration of grain boundaries. These grain boundaries will absorb the laser energy more efficiently than the grains themselves and will result in large particulates of material being ejected from the target. The particulates are transferred to the film with the same composition as the target. A similar phenomenon was observed by Arnold and Aziz,[33] who compared sintered versus solidified targets. The ablated grain boundary material from the target could account for some of the noncarbidic carbon in the HfC C 1s spectra.

Figure 3 shows the AES data from the C *KLL* region of the carbide films. The TiC spectrum, Figure 3a, shows a

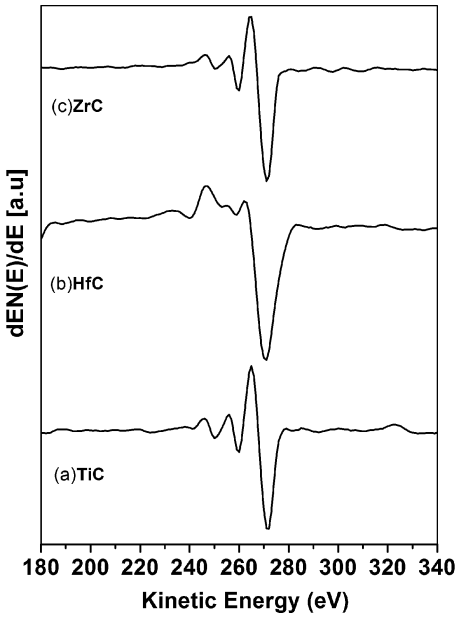

Figure 3. AES results from (a) TiC, (b) HfC, and (c) ZrC. TiC and ZrC clearly show a peak shape that is consistent with a carbide bond. HfC appears to be a combination of sp^2 and carbide-type bonds.

characteristic peak shape[34−36] for carbides. The HfC data, shown in Figure 3b, reveals a peak shape more consistent with graphitic carbon. Similar peak shapes have been shown to be the result of a combination of sp^2 and carbide[37] bonds present. The ZrC AES results, shown in Figure 3c, exhibit a similar peak shape as Figure 3a and are also consistent with a carbide[38] bond. Figure 3c shows no evidence of graphitic carbon. This is contrary to what was seen with XPS in Figure 2c. This is attributed to the fact that the XPS measurement is sampling a bigger area on the surface when compared with AES.

Figure 4 shows the XRD results of (a) TiC, (b) HfC, and (c) ZrC. All three films are polycrystalline and fit well with scans

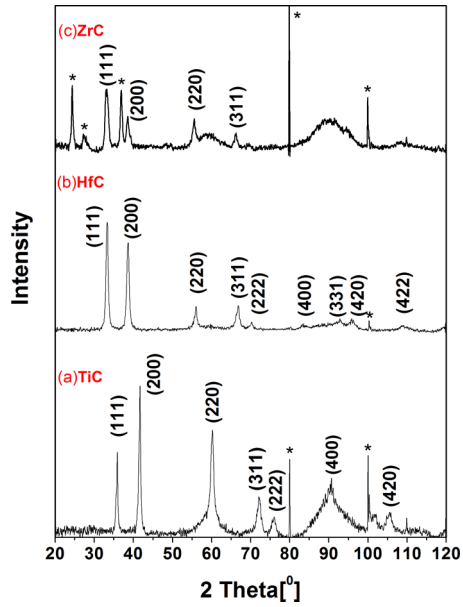

Figure 4. XRD scans of (a) TiC, (b) HfC, and (c) ZrC. Substrate peaks are indicated by *. These spectra show that all films are polycrystalline in nature and match well with database scans of stoichiometric films.

from database files of the respective TMCs.[39−41] These results show that the structure of the bulk of the films is consistent with that of stoichiometric carbides. The results from the surface analysis of all three films suggest nonstoichiometric chemistries. In the case of the HfC film, the intensity of the graphitic carbon peak in the C 1s spectra indicates another phase of carbon that is localized on the surface of the film. XRD of the HfC film in Figure 4 does not indicate that this second phase is present in the bulk of the film. This could indicate a more complex catalytic reaction on the surface of the film during ablation or possibly during the cooling to room temperature. TMCs have been shown to form graphene[42−44] layers when exposed to a hydrocarbon at high temperatures.

The TiC films were shown to be highly pure, nearly stoichiometric, and polycrystalline. On the basis of these results, a TiC film was applied to a VACNT sample under the same conditions. XPS, Auger, and UPS analysis of the film (see the Supporting Information) agreed with the previous results from the deposition of the films on planar Si. FE testing was conducted before and after the coating was applied. Figure 5 shows the results of *I*−V curve before and after the TiC coating was applied. Both curves show stable emission over the entire voltage range. The coated sample showed an order of magnitude enhancement of total current, 308 μA, when compared with that of the uncoated sample (35 μA) at 900 V.

Figure 6 shows a Fowler−Nordheim (F−N) plot of both the coated and uncoated VACNT samples. The plot was generated from the F−N equation

$$I = aV^2 e^{-b/V} \quad (1)$$

where *I* is the current in amperes, V is the voltage in volts,

$$a = 1.54 \times 10^{-6}\left(\frac{\beta^2 A_e}{\phi d^2}\right) \quad (2)$$

and

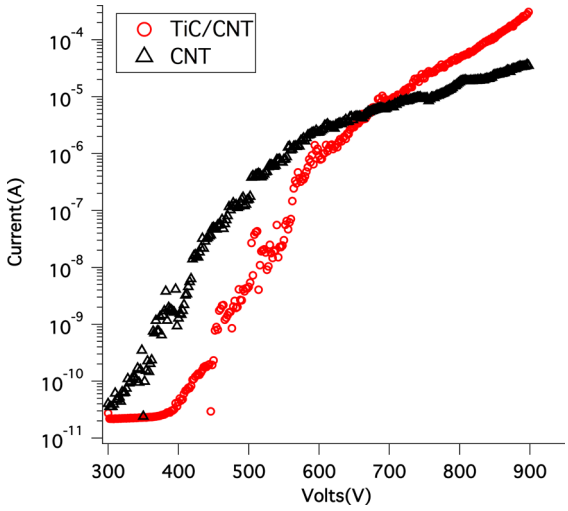

Figure 5. Field-emission results from an uncoated VACNT and TiC-coated VACNT sample. The uncoated VACNT sample had a lower turn-on voltage, 378 V, compared to the TiC/VACNT sample, 458 V. Changes in the slope demonstrate a change in the emission characteristics of both samples.

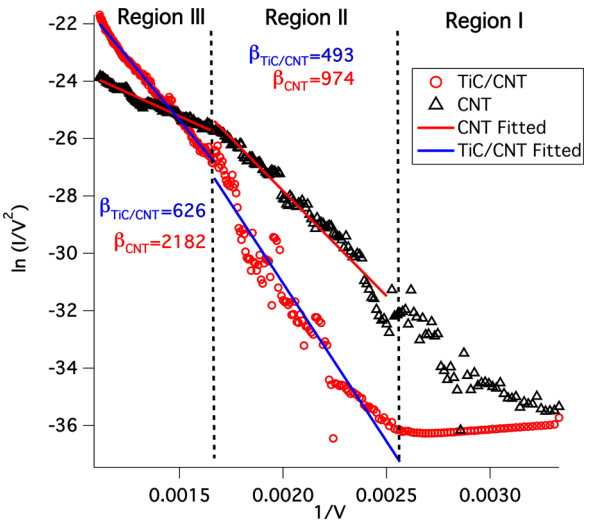

Figure 6. Fowler–Nordheim plot of TiC coated and uncoated VACNT substrates. Both samples show evidence of adsorbate-induced field emission. In both cases, emission becomes more stable with increasing field strength.

$$b = 6.8 \times 10^7 \left(\frac{\phi^{3/2} d}{\beta} \right) \tag{3}$$

For eqs 2 and 3, β is the field enhancement factor, ϕ is work function in eV, A_e is the emission area in cm^2, and d is the anode–cathode gap distance in μm. Equation 1 can be rearranged to

$$\ln \frac{I}{V^2} = \ln a - \frac{b}{V} \tag{4}$$

A plot of ln I/V^2 versus $1/V$ from eq 4 is typically used to demonstrate a linear relationship between current and voltage, thereby confirming field emission. The F–N plot in Figure 6 is broken into regions I, II, and III.[45] Region I shows that the uncoated VACNT sample has a turn-on voltage (voltage at 10^{-9} A) of about 378 V in comparison to 458 V for the TiC sample. The uncoated VACNT sample showed enhanced scatter in the emission data at lower field strengths. This same phenomena was observed for the TiC-coated VACNT in region II. In both cases, the emission began to stabilize as the field strength increased. The scatter in the data is most likely the result of adsorbates on the surface. The adsorbates desorb from the surface and mainly consist of hydrogen and carbon monoxide.[46] Both of these molecules can create surface dipoles on the surface of the cathode that have been shown to enhance emission. As the field strength increases, the adsorbates become unstable and desorb from the surface. Once most of the adsorbates are removed from the surface, the emission stabilizes to the intrinsic characteristics of the underlying substrate. Region III shows a change in slope for both samples. The TiC-coated VACNT sample showed a small change in slope for region III, which was accompanied by more stable emission. The VACNT sample shows a more drastic change in slope for region III with the emission beginning to level out.

A change in the slope of the F–N plot has a direct correlation to the field enhancement factor, β, for each sample (eq 3). Figure 6 shows the β values for both sets of conditions in rgions II and III. As expected, the β values for the coated sample are smaller than values for the uncoated VACNT. Although the TiC/VACNT sample demonstrated a slightly larger turn-on voltage when compared with an uncoated VACNT, the emission was more stable and increased steadily with increasing field strength. Becuase of the smaller change in β by a factor of 1.2 for the TiC/VACNT and 2.2 for the VACNT when going from region II to III, the TiC/VACNT sample showed that the emission of the surface was less affected by adsorbates.

A comparison with the results of Pan et al.[13] shows a 3-fold increase in total current, 308 μA, but with a coating that is 5 times as thick. Increasing the thickness of the carbide coating with negligible drop in performance is highly desired for applications involving high-power devices. A thicker coating would make the cathode more resistant to ion back-bombardment, extending the life of the cathode. The FE results also show an over 2 orders of magnitude increase in current density, 67 mA/cm^2, when compared to a similar experiment by Uh et al. (0.2 mA/cm^2)[14] and an almost a 5-fold improvement compared to Qin and Hu (14 mA/cm^2). We attribute this to the enhanced performance to the polycrystalline structure of the films.

CONCLUSIONS

These results demonstrate the advantage of the PLD technique for the application of FE cathode coatings. Previous studies involved multistep processes that resulted in amorphous carbide and carbon surfaces. Surface analysis and XRD showed that TiC films were nearly stoichiometric and polycrystalline. The FE results showed enhanced current and current density at a film thickness, 5 nm, not previously reported in the literature. A thicker film is necessary to make the field-emission cathode more resistant to ion back-bombardment. The TiC films were also shown to be less affected by adsorbates during field emission. The PLD of TiC offers a distinct advantage over other techniques in that high-quality films can be obtained under ultrahigh vacuum conditions without the use of a reactive background gas or excessively high annealing temperatures.

dx.doi.org/10.1021/am403362w | ACS Appl. Mater. Interfaces 2013, 5, 9241–9246

■ ASSOCIATED CONTENT

Supporting Information

UPS spectra of TiC-coated VACNT, Auger spectra of the VACNT before and after TiC coating, and XPS data of VACNT substrate before and after TiC coating. This material is available free of charge via the Internet at http://pubs.acs.org.

■ AUTHOR INFORMATION

Corresponding Author

*E-mail: tyson.back.ctr@wpafb.af.mil.

Notes

The authors declare no competing financial interest.

■ ACKNOWLEDGMENTS

This work was supported by AFOSR and by Air Force contract no. FA8650-11-D-5401 at the Materials and Manufacturing Directorate, AFRL/RXAP.

■ REFERENCES

(1) Senzaki, K.; Kumashiro, Y. *Jpn. J. Appl. Phys.* **1974**, *2*, 289−292.
(2) Fujii, K.; Zaima, S.; Shibata, Y.; Adachi, H.; Otani, S. *J. Appl. Phys.* **1985**, *57*, 1723−1728.
(3) Mackie, W. A.; Hartman, R. L.; Davis, P. R. *Appl. Surf. Sci.* **1993**, *67*, 29−35.
(4) Mackie, W. A.; Morrissey, J. L.; Hinrichs, C. H.; Davis, P. R. *J. Vac. Sci. Technol., A* **1992**, *10*, 2852−2856.
(5) Mackie, W. A.; Southall, L. A.; Xie, T. B.; Cabe, G. L.; Charbonnier, F. M.; McClelland, P. H. *J. Vac. Sci. Technol., B* **2003**, *21*, 1574−1580.
(6) Mackie, W. A.; Xia, T. B.; Blackwood, J. E.; Williams, S. C.; Davis, P. R. *J. Vac. Sci. Technol., B* **1998**, *16*, 1215−1218.
(7) Mackie, W. A.; Xie, T. B.; Matthews, M. R.; Routh, B. P.; Davis, P. R. *J. Vac. Sci. Technol., B* **1998**, *16*, 2057−2062.
(8) Xie, T. B.; Mackie, W. A.; Davis, P. R. *J. Vac. Sci. Technol., B* **1996**, *14*, 2090−2092.
(9) Charbonnier, F. M.; Mackie, W. A.; Hartman, R. L.; Xie, T. B. *J. Vac. Sci. Technol., B* **2001**, *19*, 1064−1072.
(10) Charbonnier, F. M.; Mackie, W. A.; Xie, T.; Davis, P. R. *Ultramicroscopy* **1999**, *79*, 73−82.
(11) Mackie, W.; Hinrichs, C. H. *J. Cryst. Growth* **1988**, *87*, 101−106.
(12) Deheer, W. A.; Chatelain, A.; Ugarte, D. *Science* **1995**, *270*, 1179−1180.
(13) Pan, L.; Shoji, T.; Nagataki, A.; Nakayama, Y. *Adv. Eng. Mater.* **2007**, *9*, 584−587.
(14) Uh, H. S.; Park, S.; Kim, B. *Diamond Relat. Mater.* **2010**, *19*, 586−589.
(15) Qin, Y. X.; Hu, M. *Appl. Surf. Sci.* **2008**, *254*, 3313−3317.
(16) Shirley, D. A. *Phys. Rev. B: Condens. Matter Mater. Phys.* **1972**, *5*, 4709−4714.
(17) Savitzky, A.; Golay, M. J. E. *Anal. Chem.* **1964**, *36*, 1627−1639.
(18) Amama, P. B.; Pint, C. L.; McJilton, L.; Kim, S. M.; Stach, E. A.; Murray, P. T.; Hauge, R. H.; Maruyama, B. *Nano Lett.* **2008**, *9*, 44−49.
(19) Santerre, F.; El Khakani, M. A.; Chaker, M.; Dodelet, J. P. *Appl. Surf. Sci.* **1999**, *148*, 24−33.
(20) Zaima, S.; Adachi, H.; Shibata, Y. *J. Vac. Sci. Technol., B* **1984**, *2*, 73−78.
(21) Rist, O.; Murray, P. T. *Fresenius' J. Anal. Chem.* **1991**, *341*, 360−364.
(22) Luthin, J.; Linsmeier, C. *Surf. Sci.* **2000**, *454*, 78−82.
(23) Lewin, E.; Gorgoi, M.; Schäfers, F.; Svensson, S.; Jansson, U. *Surf. Coat. Technol.* **2009**, *204*, 455−462.
(24) Magnuson, M.; Lewin, E.; Hultman, L.; Jansson, U. *Phys. Rev. B: Condens. Matter Mater. Phys.* **2009**, *80*, 235108-1−235108-7.
(25) Zhang, J. H.; Yang, C. R.; Wang, Y. J.; Feng, T.; Yu, W. D.; Jiang, J.; Wang, X.; Liu, X. H. *Nanotechnology* **2006**, *17*, 257−260.
(26) Suzuki, S.; Bower, C.; Kiyokura, T.; Nath, K. G.; Watanabe, Y.; Zhou, O. *J. Electron Spectrosc. Relat. Phenom.* **2001**, *114−116*, 225−228.
(27) Ishiwawa, Y. *Electric Refractory Materials*; Marcel Dekker: New York, 2000.
(28) Gruzalski, G. R.; Zehner, D. M.; Noonan, J. R.; Davis, H. L.; Didio, R. A.; Muller, K. *J. Vac. Sci. Technol., A* **1989**, *7*, 2054−2059.
(29) Poirier, D. M.; Weaver, J. H. *Surf. Sci. Spectra* **1993**, *2*, 232−241.
(30) Rooke, M. A.; Sherwood, P. M. A. *Carbon* **1995**, *33*, 375−380.
(31) Guo, B. C.; Wei, S.; Purnell, J.; Buzza, S.; Castleman, A. W. *Science* **1992**, *256*, 515−516.
(32) Cartier, S. F.; Chen, Z. Y.; Walder, G. J.; Sleppy, C. R.; Castleman, A. W. *Science* **1993**, *260*, 195−196.
(33) Arnold, C. B.; Aziz, M. J. *Appl. Phys. A: Mater. Sci. Process.* **1999**, *69*, S23−S27.
(34) Coad, J. P.; Riviere, J. C. *Surf. Sci.* **1971**, *25*, 609−624.
(35) Grant, J. T.; Haas, T. W. *Surf. Sci.* **1971**, *24*, 332−334.
(36) Haas, T. W.; Grant, J. T. *Appl. Phys. Lett.* **1970**, *16*, 172−173.
(37) Lahiri, J.; Batzill, M. *Appl. Phys. Lett.* **2010**, *97*, 023102-1−023102-3.
(38) Craciun, V.; Woo, J.; Craciun, D.; Singh, R. K. *Appl. Surf. Sci.* **2006**, *252*, 4615−4618.
(39) *Powder Diffraction File No. 03-065-8747*, 2 Release 2007; International Centre for Diffraction Data: Newton, PA.
(40) *Powder Diffraction File No. 00-032-1383*, 2 Release 2007; International Centre for Diffraction Data: Newton, PA.
(41) *Powder Diffraction File No. 01-089-4054*, 2 Release 2007; International Centre for Diffraction Data: Newton, PA.
(42) Aizawa, T.; Souda, R.; Otani, S.; Ishizawa, Y.; Oshima, C. *Phys. Rev. B: Condens. Matter Mater. Phys.* **1990**, *42*, 11469−11478.
(43) Nagashima, A.; Nuka, K.; Itoh, H.; Ichinokawa, T.; Oshima, C.; Otani, S. *Surf. Sci.* **1993**, *291*, 93−98.
(44) Yu, M. L.; Hussey, B. W.; Kratschmer, E.; Chang, T. H. P.; Mackie, W. A. *J. Vac. Sci. Technol., B* **1995**, *13*, 2436−2440.
(45) Dean, K. A.; von Allmen, P.; Chalamala, B. R. *J. Vac. Sci. Technol., B* **1999**, *17*, 1959−1969.
(46) Murray, P. T.; Back, T. C.; Cahay, M. M.; Fairchild, S. B.; Maruyama, B.; Lockwood, N. P.; Pasquali, M. *Appl. Phys. Lett.* **2013**, *103*, 053113-1−053113-4.